Highly charged ruthenium(II) polypyridyl complexes as effective photosensitizer in photodynamic therapy

Luca Conti, [a]* *Andrea Bencini,* [a] *Camilla Ferrante,* [b] *Cristina Gellini,* [a] *Paolo Paoli,* [c] *Matteo Parri,* [c] *Giangaetano Pietraperzia,* [a] *Barbara Valtancoli,* [a] *and Claudia Giorgi* [a] *

[a] Department of Chemistry '*Ugo Schiff*,' Via della Lastruccia 3, 50019, Sesto Fiorentino (FI), Italy

[b] Department of Chemical Sciences and UR INSTM, University of Padova, via Marzolo 1, 35131, Padova (PD), Italy

[c] Dipartimento di Scienze Biomediche, Sperimentali e Cliniche "Mario Serio", Università degli Studi di Firenze, Via Viale Morgagni 50, Firenze (FI), Italy

KEYWORDS: Photodynamic therapy, ruthenium(II) polypyridyl complexes, DNA interaction, singlet oxygen, ROS.

ABSTRACT. A comparative study between two novel mixed ligand ruthenium(II) polypyridyl complexes, [Ru(phen)$_2$**L'**] and [Ru(phen)$_2$Cu(II)**L'**] (**L** and **L**-Cu(II)) (scheme 1), featuring the peculiar polyaazamacrocyclic unit 4,4'-(2,5,8,11,14-pentaaza[15])-2,2'-bipyridilophane (**L'**), is

herein reported. Thanks to the presence of the inserted polyaazamacrocyclic moiety, **L** is capable to bind metal ions (namely Zn(II) and Cu(II)) in aqueous media and both **L** and **L**-Cu(II) feature a high solubility in water. Following the study of the capacity of these to produce $^1O_2$ upon irradiation, we investigated their ability to interact with ct-DNA and to damage the biopolymer when activated by light. Both **L** and **L**-Cu(II) were found to efficiently photocleave the DNA plasmid under light irradiation. The complexes also possess a marked light-induced cytotoxicity, as revealed by a study on a A375 human melanoma cell line. In particular, the higher light-triggered biological activity of **L**-Cu(II) with respect to **L** suggests that the Fenton active copper ion in the mixed Ru(II)/Cu(II) specie plays a synergetic role with light activation in the formation of citotoxic ROS species, thus providing an alternative pathway for damaging biological targets. In addition, the Ru(II) complexes, even in the presence of Cu(II), can be visualized in cellular compartments exploiting the classic luminescence of Ru(II) complexes with polypyridine ligands.

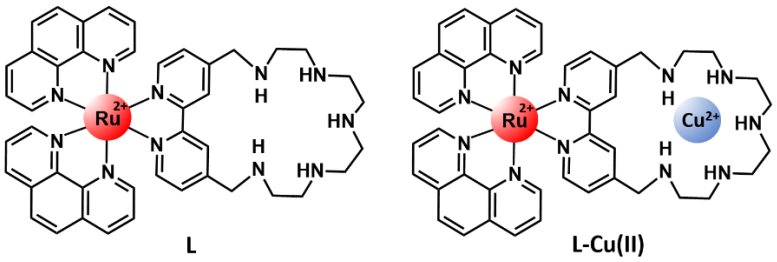

Scheme 1. Schematic representation of **L** and **L**-Cu(II).

INTRODUCTION

In recent years, photodynamic therapy (PDT) has received increasing attention due to the encouraging responses of its application in the treatment of a wide variety of cancers, including lung, bladder, esophageal and skin tumors, as well as in bacterial infections.[1,2,3,4]

PDT relies on the use of a photosensitizer agent (PS), that can be triggered by irradiation with low-energy light to generate cytotoxic species, such as reactive oxygen species (ROS), thus providing a complete spatial and temporal control over the generation of the toxic molecule.[5] Generally, light-activated PSs can react with the molecular oxygen leading to the formation of ROS through two distinct pathways. In accordance with a Type I reaction, the triplet excited state of the PS can determine a direct electron or proton transfer to the surrounding biological substrates, inducing the formation of radicals that can further interact with molecular oxygen to form ROS, such as superoxide, hydroxyl radicals or peroxides. In Type II mechanisms an energy transfer from the triplet excited state of the PS to ground-state molecular oxygen ($^3O_2$) can occur, bringing to the production of extremely cytotoxic singlet oxygen ($^1O_2$). This specie, with an estimated half-life of 40 ns in a biological environment,[6] represents a very reactive form of oxygen and can rapidly react with biological targets, determining topical oxidative damages that can ultimately induce the cellular death.

The light-induced production of $^1O_2$ plays a key role in the development of PS for PDT. In fact, the great majority of the PSs that are currently applied in clinics mainly rely on Type II mechanism,[7,8] and are based on cyclic tetrapyrrolic scaffolds, namely phorphirins,

phthalocyanins, and chlorins.[9] However, the performances of these molecules are often limited by important disadvantages, such as low solubility in biological media, scarce selectivity and pro-longed patient photosensitivity, as in the case of Photofrin®, used for the treatment of lung and esophageal cancers.[10] As consequence, many efforts have been undertaken to move away from tetrapyrrolic systems, making appealing the exploration of transition metal complexes as potential PDT agents. In this context, ruthenium(II) polypyridil complexes are attracting much interest due to the rich photoluminescence repertoire, DNA binding ability, redox chemistry, and tunable absorption properties.[11,12,13,14] In particular, their ^{3}MLCT (metal to ligand charge transfer) state can be easily quenched by molecular oxygen to generate singlet oxygen with good quantum yields, as in the case of $[Ru(bpy)_3]^{2+}$ (bpy = 2,2'-bipyridine), that showed a great ability to induce apoptosis of cancer cells in presence of light, although the scarce selectivity and low DNA binding affinity limited its further application as PDT agent.[15] One of the most important class of anticancer drugs among ruthenium(II) polypyridyl complexes, is represented by DNA intercalators. The versatility of such compounds rely on the possibility to vary the nature of the substituent group in the intercalative ligand, modifying the configuration and electron density distribution of the metal center, allowing to obtain different DNA binding affinities and photo-cleavage properties. Following this approach, a considerable number of compounds have been reported, including $[Ru(bpy)_2(dppz)]^{2+}$ and $[Ru(bpy)_2(pip)]^{2+}$ (dppz = dipyridophenazine, pip = 2-phenylimidazo[4,5-f][1,10]phenanthroline), which feature interesting properties as site-specific luminescent DNA binding agents and abilities to stall the DNA replication of cancer cells as well.[16] However, some critical disadvantages, such as the short lifetime of triplet excited state that reduces the $^1O_2$ quantum yield, the low DNA cleavage activity and the scarce solubility in physiological media, may represent a serious limit for their further development as PSs in

clinical trials.[17] In this context, Ru-polypyridyl complexes with charged chains appended to the heteroaromatic units represent an appealing choice, although, to the best of our knowledge, they have not been largely investigated as PDT photosensitizer .[18-19-20]

In the present work, we report on two novel ruthenium(II) polypyridyl complexes, $[Ru(phen)_2\mathbf{L'}]$ and $[Ru(phen)_2Cu(II)\mathbf{L'}]$ (**L** and **L**-Cu(II)), containing the peculiar polyamine macrocyclic unit **L'**(**L'** = 4,4'-(2,5,8,11,14-pentaaza[15])-2,2'-bipyridilophane).

The presence of five amino groups on **L'**, which can easily undergo protonation in water, confers to Ru(II) compounds a high water solubility and to **L** the capability to bind important physiological ions in aqueous media, namely zinc(II) and copper(II). Following the potentiometric analysis of the protonation/metal binding equilibria of **L**, the capacity of Ru(II) compounds to generate $^1O_2$ upon irradiation was determined by fluorescence excited state measurements. Uv-visible and fluorescence titrations were performed in order to assess the interaction of such complexes with ct-DNA, while gel electrophoresis experiments were conducted to establish their ability to cleave the biopolymer when light-activated. Finally, we compared their photo-induced biological potential on a A375 human melanoma cell line.

RESULTS AND DISCUSSION

Synthesis. **L** and **L**-Cu(II) were obtained as described in the experimental following the synthetic strategy shown in scheme 2. The intermediate $(phen)_2RuCl_2$ was prepared accordingly with the methods described in literature,[21,22] by reaction of $RuCl_3 \cdot xH_2O$ with two equivalents of 1,10-phenanthroline in the presence of an excess of LiCl in anhydrous DMF. The following step consisted in the direct reaction of $(phen)_2RuCl_2$ with the bidentate **L'** ligand in ethylene glycol, under microwave irradiation.

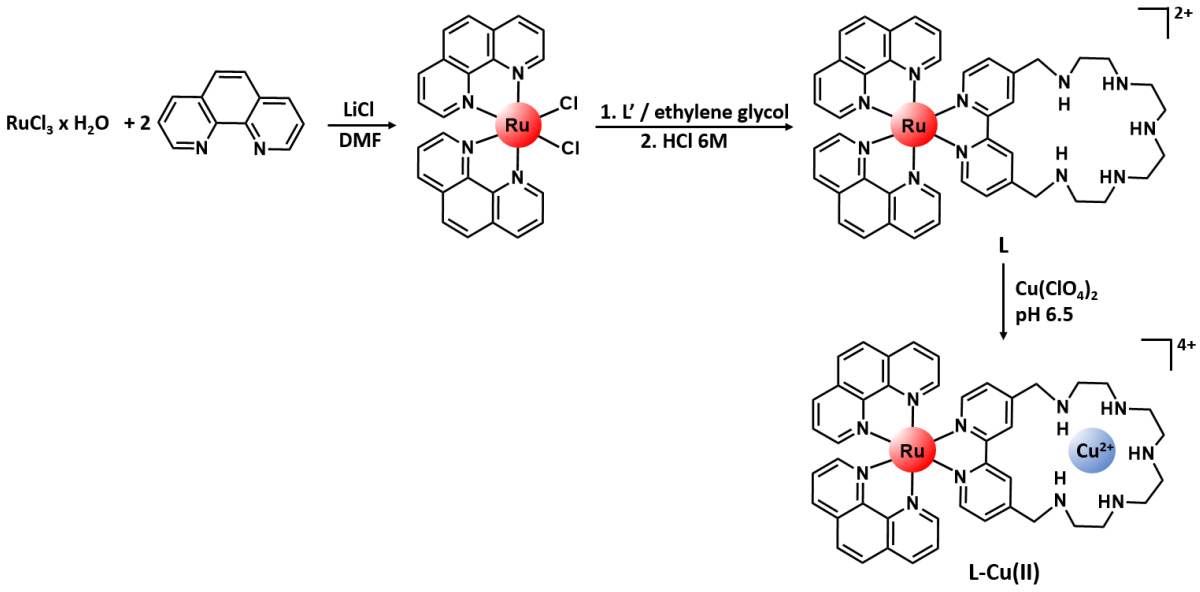

Scheme 2. Synthetic route for preparation of complex **L**

With respect to conventional heating methods, the use of the microwave assisted technology permits to improve the yield of the compound and effectively reduces the reaction time.[23,24] In

our case in fact, **L** was formed after heating the reaction mixture at 160 °C for only 7 minutes. We can assume that this process is also facilitated by the lability of the two chloride ligands, which allows their replacement by the bidentate ligand **L'**. Finally, treatment of **L** with an equimolar amount of $Cu(ClO_4)_2$ at pH 6.5 afforded to obtain the correspondent **L**-Cu(II) complex directly from the aqueous solution.

Protonation properties of L. As previously mentioned, the polyamine chain **L'** in **L**, can easily protonate in aqueous solution affording highly charged polyamminum cations and thus making fundamental the preliminary study of the protonation equilibria of **L**. To this aim, we started studying the protonation equilibria of **L** by means of potentiometric measurements in NaCl 0.1 M at 298 ± 0.1 K. The resulting protonation constants are reported in table 1, together with the distribution diagram of the species present solution (figure S1, ESI). The compound acts as a pentaprotic base, with the $[H_3\mathbf{L}]$ specie being the most abundant at neutral pH values. The protonation constants appear to be similar to those previously found for the analogous bipyridyl compound $[(bpy)_2Ru\mathbf{L'}]^{2+}$,[25] and consistent with the foreseen protonation pattern for aliphatic polyamine macrocycles.[26,27] However, **L** displays a lower basicity, in each protonation step, with respect to the free macrocyclic unit **L'**, probably due to the electrostatic repulsion between the Ru(II) center and the positively charged polyammonium residues.

Table 1. Protonation constants of **L** determined by means of potentiometric measurements in NaCl 0.1 M, at 298.1 ± 0.1 K. Values in parentheses are standard deviations in the last significant figure. ([**L**] = 1 x 10^{-3} M).

reaction	logK
$\mathbf{L}^{2+} + H^+ = H\mathbf{L}^{3+}$	8.90 (5)
$H\mathbf{L}^{3+} + H^+ = H_2\mathbf{L}^{4+}$	8.01 (6)
$H_2\mathbf{L}^{4+} + H^+ = H_3\mathbf{L}^{5+}$	5.32 (5)
$H_3\mathbf{L}^{5+} + H^+ = H_4\mathbf{L}^{6+}$	3.93 (5)

$$H_4\mathbf{L}^{6+} + H^+ = H_5\mathbf{L}^{7+} \qquad 2.44\ (6)$$

A further investigation of the proton binding ability of **L** was carried out by means of spectrophotometric and spectrofluorimetric measurements. The UV-vis spectra of the ruthenium complex recorded in aqueous media at different pH values are reported in figure S2 (ESI). The absorption spectra display a broad band at about 450 nm, which can be attributed to a metal-to-ligand dπ-π* charge transfer (MLCT) and a structured band centered at lower wavelengths (~ 270 nm), due to the ligand centered π-π* transitions of the phenanthroline units. As shown in figure S2, the absorption properties of the compound do not change significantly with pH, revealing a scarce influence of the protonation state of the polyamine moiety on its absorption features.[28]

In contrast with the absorption, the fluorescence emission of **L** is markedly affected by pH. In fact, as shown in figure 1, a marked quenching of the emission is observed as the pH decrease from 11 to 2.5, together with a red shift of the emission band, which is 25 nm red-shifted at pH 2 with respect to pH 12.

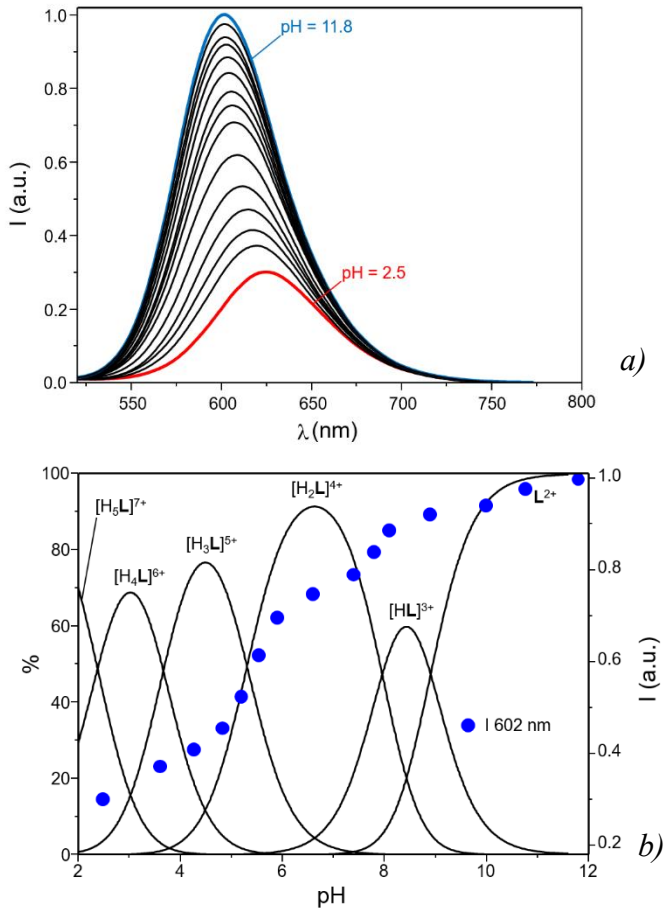

Figure 1. a) Emission spectra of **L** at different pH values. b) Variation of the fluorescence emission at 602 nm as a function of pH, overlapped with the distribution diagram of the protonated species present in solution. [**L**] = 1 x 10^{-5} M, λ_{exc} = 411 nm.

Most likely, the quenching of luminescence observed by lowering the pH could be explained with the increase in the protonation state of the polyamine macrocyclic moiety. The consequent formation of a more distorded excited-state geometry of the molecule, which favors radiationless processes, might be responsible for the poor emissive species revealed for low pH values. Furthermore, a higher protonation state of the receptor unit might also lead to the formation of a better electron acceptor, lowering the energy of the MLCT and thus justifying the increase in the Stokes shift observed.

Binding ability of L towards cationic substrates. The polyamine unit linked to the complexed Ru(II) center of **L** appears to be a promising binding site for metal ions. For that reason we investigated the binding capacity of **L** towards Zn(II) and Cu(II), by means of potentiometric titrations. The species formed and their stability constants are listed in table 2, while the correspondent distribution diagrams of the species present in solution are reported in figures S3-S5 (ESI).

Table 2. Complexation constants of **L** with Zn(II) and Cu(II) determined by means of potentiometric measurements in NaCl 0.1 M, at 298.1 ± 0.1 K. Values in parentheses are standard deviations in the last significant figure. ([**L**] = 1 x 10^{-3} M).

reaction	logK	
	Zn(II)	Cu(II)
$\mathbf{L}^{2+} + M^{2+} = M\mathbf{L}^{4+}$	8.09 (8)	15.12 (6)
$M\mathbf{L}^{4+} + H^{+} = [HM\mathbf{L}]^{5+}$	7.17 (6)	5.63 (7)
$[HM\mathbf{L}]^{5+} + H^{+} = [H_2M\mathbf{L}]^{6+}$	5.56 (8)	3.94 (7)
$[H_2M\mathbf{L}]^{6+} + H^{+} = [H_3M\mathbf{L}]^{7+}$	4.75 (8)	
$M\mathbf{L}^{4+} + OH^{-} = [M\mathbf{L}(OH)]^{3+}$		6.12 (9)
$M\mathbf{L}^{4+} + 2OH^{-} = [M\mathbf{L}(OH)_2]^{2+}$	11.55 (9)	
$\mathbf{L}^{2+} + 2M^{2+} + OH^{-} = [M_2\mathbf{L}(OH)]^{5+}$		12.71 (8)

As shown in table 2 and figures S3 and S4 (ESI), **L** displays a high tendency to form stable mononuclear complexes with both Zn(II) and Cu(II) in a wide range of pH (2.5-11). Furthermore, in the case of Cu(II), the formation of binuclear complexes was also observed. The stability constants determined for the complexation of **L** with Zn(II) and Cu(II) are slightly lower relative to those reported for the free macrocycle **L'**.[29] As expected in fact, **L'** displays a reduced coordination ability towards metal ions when its bipyridyl moiety is linked to Ru(II), due to the electrostatic repulsion between the ruthenium center and the positively charged guest ion.

The UV-vis absorption spectra of **L** does not significantly change upon Cu(II) binding (figure S6, ESI). Conversely, the luminescence emission spectra are strongly affected by Cu(II) binding.

Cu(II) complexation, in fact, induces a remarkable quenching of the emission, as expected considering the paramagnetic nature of this metal cation.[30] In case of Zn(II) binding instead, both the UV-vis and fluorescence emission spectra are only slightly affected by the metal coordination, with the emission being only 15% decreased in the presence of 1 eq. of the metal (Figures S6-S7a, ESI).

Interaction of Ru(II) complexes with ct-DNA

Absorption measurements. Electronic absorption spectroscopy represents a useful technique to probe the DNA interaction of metal-complexes. In fact, while base binding is generally associated to a perturbation of the ligand field transition of the metal complex, the intercalative mode of interaction usually determines hypochromism and batochromism in the MLCT band, with the extent of hypochromism directly linked to the intercalative binding strength. Moreover, metal complexes could also interact with DNA via partial intercalative or electrostatic mode, resulting in either hyperchromism or hypochromism.[31,32]

In this context, we investigated the interaction of **L** and **L**-Cu(II) with ct-DNA by monitoring the changes of their absorption spectra in Tris-HCl buffer at 298 K, upon addition of increasing amounts of the biopolymer to solutions of Ru(II) complexes at fixed concentration.

As shown in Figure 2a, addition of DNA to a solution of **L** induces the hypochromism at the MLCT band of the complex, whose absorbance at 452 nm is reduced of ca 35%, in the presence of 200 μM of ct-DNA.

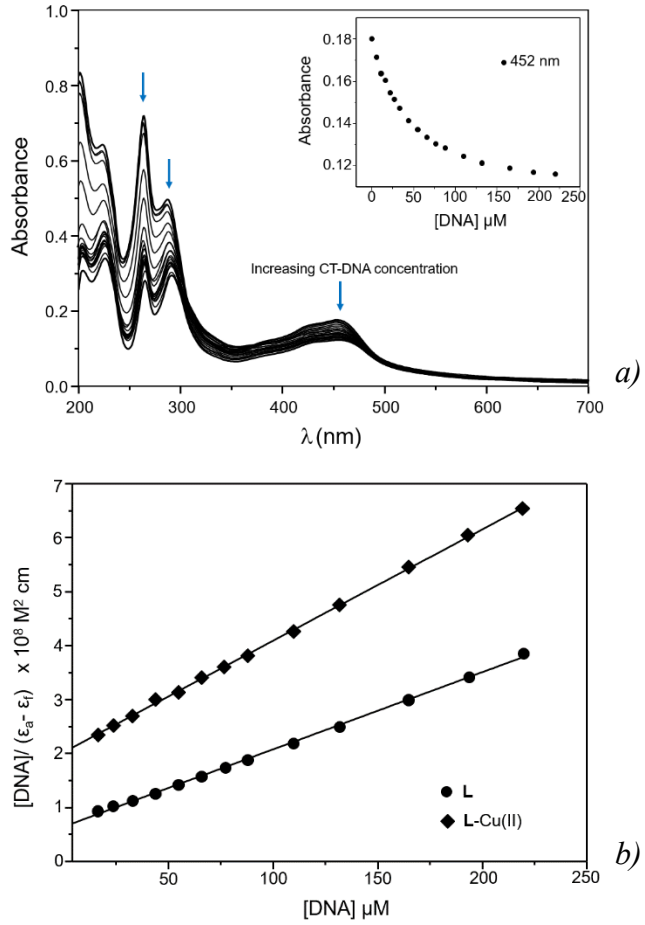

Figure 2. a) Absorption spectra of **L** in Tris-buffer 10 mM, (NaCl 50 mM, pH 7.2) in presence of increasing amounts of calf thymus DNA. The inset shows the absorbance at 542 nm as a function of the DNA concentration. b) Plots of [DNA]/($\varepsilon_a - \varepsilon_f$) versus [DNA] obtained from UV titration of **L** and **L**-Cu(II) with ct-DNA. ([**L**] = [**L**-Cu(II)] = 11µM, [ct-DNA] = 0-220 µM).

Similar results were also observed in the case of **L**-Cu(II) (Figure S8), although the extent of hypochromism was less intense with respect to **L** (ca 21 % at 452 nm, 200 µM of DNA). In both cases, no blue or red shift was observed upon DNA addition.

To further study the affinity of these complexes with the biopolymer, their intrinsic binding constants K_b towards ct-DNA were determined, as described in ESI. K_b values for **L** and **L**-Cu(II) with ct-DNA were found to be (2.77 ± 0.07) x 10^4 M^{-1} and (1.47 ± 0.01) x 10^4 M^{-1}

respectively, while the correspondent plots of [DNA]/($\varepsilon_a - \varepsilon_f$) versus [DNA] are reported in Figure 2b.

Of note, the obtained constants result to be slightly higher with respect to that of the parent compound $[Ru(phen)_3]^{2+}$(< 10^3 M^{-1} in the same buffered media),[33,34] which has been reported to interact with ct-DNA mainly *via* non-classical intercalation processes, namely *semi*-intercalation, *quasi*-intercalation and external electrostatic binding mode in the major groove of the biopolymer.[35,36] On the other hand, these values are ca. 2 order of magnitude lower than those reported for classical ruthenium based intercalators, such as $[Ru(phen)_2(dppz)]^{2+}$,[37,38] thus indicating that a pure intercalative binding of DNA can be ruled out.

We also point out that the intrinsic binding constant obtained for **L**-Cu(II) results to be almost 2-fold lower with respect to that of **L**, as also shown by the intercept values of the plot of [DNA]/($\varepsilon_a - \varepsilon_f$) versus [DNA] reported in Figure 2b.

This may evidence the central role of the electrostatic and/or hydrogen bonding interactions between the protonated polyamine chain of **L** and the DNA backbone. In particular, we can reasonably speculate that positively charged ammonium groups on **L'** could interact with the biopolimer via electrostatic and hydrogen bonding interactions with DNA phosphate groups, justifying the greater K_b value of **L** relative to that of classical parent compounds, such as $[Ru(phen)_3]^{2+}$. In contrast, when a copper ion is bound within the macrocyclic cavity, the nitrogen donor atoms would be less available for electrostatic interaction with the DNA phosphate backbone. In addition, the copper center is likely to be almost coordinatively saturated by the macrocyclic amine groups, precluding its potential interaction with phosphate and thus explaining the lower K_b value of the Cu(II) complex with respect to **L**.

Fluorescence measurements. Luminescence titration experiments were also carried out, and the emission spectra for **L** in the absence and in presence of increasing concentrations of ct-DNA are reported in figure 3-a. Unfortunately, the scarce fluorescence emission of **L**-Cu(II) prevents the analogue study on the Cu(II) complex.

As shown in figure 3 a-b, the complex undergoes a sharp quenching of its luminescence in presence of low [DNA] concentrations ([DNA]/[Ru] < 1) whereas, upon increasing the [DNA]/[Ru] ratio (> 1), its fluorescence emission is restored, resulting blue shifted of almost 12 nm with respect to that of the ligand in absence of DNA (inset of figure 3-a). No significant variations were recorded above [DNA]/[Ru] ratios of 20. Of noting, the dependency of the fluorescence intensity of ligand on the oligonucleotide concentration is remarkably different with respect to that reported in literature for the parent compound $[Ru(phen)_3]^{2+}$, which exhibits a linear enhancement of fluorescence with increasing DNA concentrations.[39] This may suggest the occurrence of different mechanisms of interaction of **L** with ct-DNA, depending on the range of [DNA]/[Ru] ratios involved. However, in analogy with that reported for $[Ru(phen)_3]^{2+}$ and for classical intercalative polypyridyl Ru(II) complexes, we can speculate that the increase of emission at [DNA]/[Ru] molar ratios > 1 might be due to the reduction on the accessibility of solvent molecules to the ligand. In these conditions in fact, the ligand mobility is restricted to the DNA binding site, causing a lowering of the sensitivity to emission-quenching processes by collision with solvent molecules and thus leading to the enhancement of the fluorescence emission of the ruthenium complex. On the other hand, in the presence of low DNA concentrations ([DNA]/[Ru] < 1), we can reasonably assume the involvement of the ruthenium complex in weaker interactions with the biopolimer, as weak groove DNA-binding modes, possibly responsible of the initial quenching effect observed.[40]

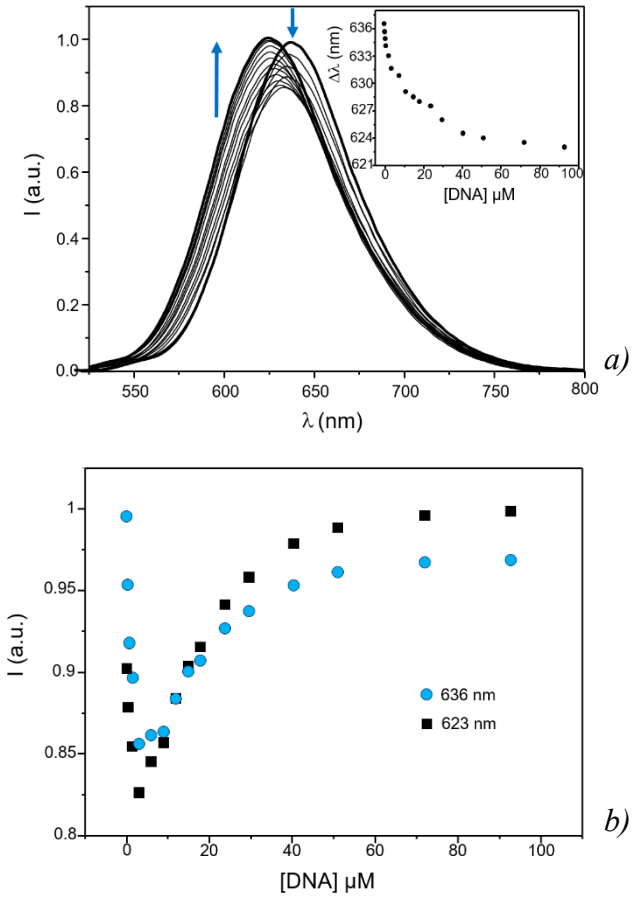

Figure 3. a) Emission spectra of **L** in Tris-HCl buffer in the absence and presence of increasing amounts of calf thymus DNA. The inset of top right of the figure shows the variation (blue shift) of the wavelength corresponding to the maximum fluorescence emission of **L** with increasing DNA concentrations. b) Variation of the fluorescence emission of **L** at 623 and 636 nm as a function of increasing concentration of the biopolymer. [**L**] = 3 μM, [CT-DNA] = 0-100 μM, λ_{exc} = 411 nm, (10 mM Tris-HCl, 50 mM NaCl, pH 7.2).

With the aim of further investigate the DNA interaction of **L**, we performed steady-state emission quenching experiments using ferrocyanide ($[Fe(CN)_6]^{4-}$) as anionic quencher (Q).

Figure 4 shows the Stern-Volmer plot for the luminescence quenching of the ruthenium complex alone and bound to DNA ([DNA]/[Ru] = 20), in the presence of increasing concentration of ferrocyanide. In the absence of DNA, **L** is efficiently quenched by ferrocyanide anions and

shows a linear Stern Volmer plot, as expected for a single component donor-quencher system. From the slope of the plot of F_o/F versus [Q], and by using the linear equation described in the experimental, we obtained a K_{sv} value of (11.55 ± 0.06) x 10^4 M^{-1}, in good agreement with K_{sv} values reported in literature for luminescent systems whose fluorescence quenching is mainly attributed to electrostatic interactions with quencher molecules.[41]

In presence of DNA, the quenching of fluorescence emission of the ligand induced by addition of ferrocyanide anions is drastically reduced with respect to free Ru(II) compound, revealing a high affinity between the complex and DNA. Furthermore, and contrary to the system in the absence of the biopolimer, the Stern-Volmer plot results biphasic and a downward curvature was observed (see inset of the figure 4). For that reason, data were analyzed by using a modified form of equation 2, (eq. 1, ESI), accordingly with the approach followed by Eftink and Selvidge[42]: the correspondent parameters are reported in Table 1 of supporting information. The strong decrease of K_{sv} value from (11.55 ± 0.06) x 10^4 M^{-1} to (2.60 ± 0.13) x 10^3 M^{-1} in the presence of DNA (Table 1, ESI), confirms the efficient shielding of **L** from the quencher molecules, due to the electrostatic repulsion between the polyanionic backbone of DNA and the highly negatively charged ferro-cyanide anions.Moreover, the downward curvature observed in the presence of DNA may be explained with the presence in solution of two distinct populations of Ru(II) complexes, featuring different chemical surroundings. [42]

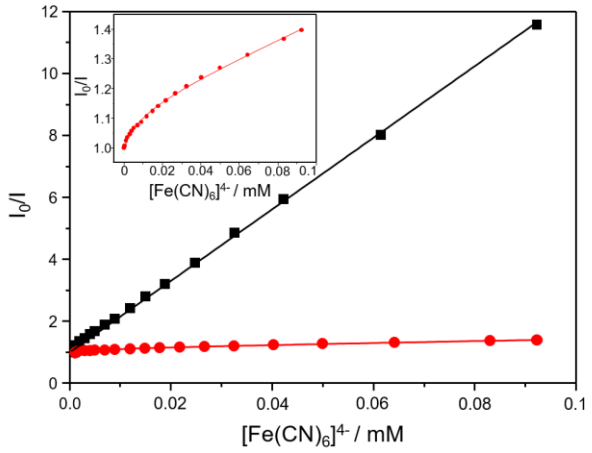

Figure 4. Ster-Volmer plots for the quenching of fluorescence of free (black squares) and DNA-bound (red circles) complex **L** with $[Fe(CN)_6]^{4-}$. On top left of the figure is shown a magnification of the Stern-Volmer plot for **L**-DNA system. [**L**] = 3 μM, [DNA]/[Ru] = 40, λ_{exc} = 411 nm, λ_{em} = 634 nm.

Excited state lifetimes measurements. With the aim of deeper investigate the different Ru(II) chemical environments observed in the presence of DNA, excited state lifetimes measurements of L in absence and in the presence of ct-DNA at a ratio [**L**]/[DNA] of 1:20, were performed and the corresponding emission decay profiles are reported as a function of time in figure 5. In absence of DNA, the fluorescence decay curve fits well with a mono-exponential decay functional form, resulting in a lifetime of τ_1 = 375.8 ± 1.4 ns with a R^2 = 0.99879. Upon binding of ct-DNA, the complex exhibits a bi-exponential decay, featuring two distinct fluorescence decay times, τ_1 = 73.7 ± 1.3 ns and τ_2 = 606.3 ± 3.3 ns, with a R^2 = 0.99965.

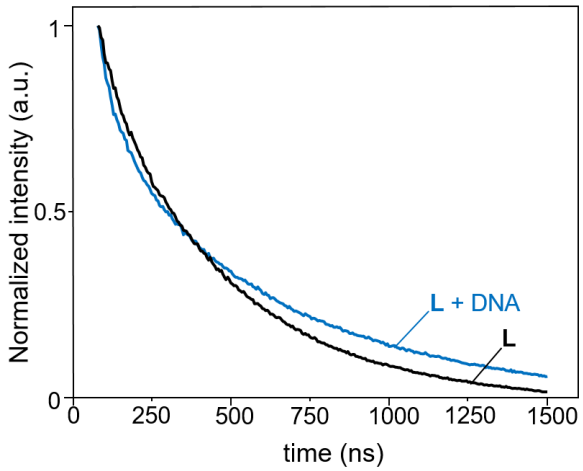

Figure 5. Emission decay profile vs. time for complex **L** in Tris-HCl buffer in the absence (black line) and presence (blue line) of CT -DNA ([**L**] = 50 μM, [DNA]/[**L**] = 20).

The longer lifetime found in the presence of the biopolymer is almost 30% lower than that reported for classical intercalating Ru(II) complexes, such as $[Ru(phen)_2DPPZ]^{2+}$ (ca. 800 ns),[43] ruling out the occurrence of a pure intercalative interaction mode, in agreement with the spectroscopic and fluorescence titrations discussed above.

In addition, the origin of a bi-exponential decay curve, characterized by two fluorescence lifetimes, indicates the presence of two DNA bound ruthenium species, featuring different solvent accessibilities.

In particular, we can speculate that the polynucleotide may provide an hydrophobic cavity for the ruthenium compound preventing its luminescence quenching by water molecules. This process would be namely due to a partial insertion of a phenantroline unit into the major/minor groove of DNA,[44] justifying the longer lifetime component of the luminescence decay. On the other hand, the shorter lifetime component may be attributed to the electrostatic interaction between the positively charged polyammonium chain of L and the negative phosphate groups on the DNA

backbone, which determines a greater exposure of the metal center of complex to solvent molecules.[45,46]

Singlet oxygen generation. A quantitative assessment of the singlet oxygen $^1O_2$ produced by ruthenium-based systems upon light irradiation was performed to investigate the potential of such compounds as PS agents in PDT. To this aim, the phosphorescence signals of $^1O_2$ at 1270 nm induced by irradiation of compounds at 400 nm in air-saturated CH_3CN solutions were measured. The correspondent $^1O_2$ quantum yields (ϕ_Δ) were evaluated by comparison with the reference molecule tetraphenylporphyrin (TPP), as described in the experimental section. The resulting values are reported in Table 3. As shown, the $^1O_2$ quantum yield (ϕ_Δ) determined for **L** was found to be 0.29 ± 0.06. This value is comparable with that measured for the parental compound $Ru(phen)_3^{2+}$ under the same experimental conditions (ϕ_Δ = 0.38 ± 0.06), thus indicating that the substitution of a phenantroline unit with the bipyridyl chelating moiety of **L'** does not significantly affect the capacity of the complex to produce $^1O_2$. On the contrary, in case of **L**-Cu(II) no $^1O_2$ emission was detected under these experimental conditions. Quenching of the fluorescence emission of the MLCT state of **L** upon binding Cu(II) together with the lack of evidence for $^1O_2$ production, can be explained by supposing that the decay of the MLCT state of **L**-Cu(II) occurs mainly through internal conversion and likely on a faster timescale with respect to **L**.

Table 3. Excited state life-time values obtained by fluorescence measurements together with the $^1O_2$ quantum yields (ϕ_Δ) determined in air-saturated CD_3CN solutions.

	τ_1 (ns)	τ_2 (ns)	$\tau_1 : \tau_2$	ϕ_Δ
Free **L**	375.8 ± 1.4			0.29 ± 0.06
L / DNA	73.7 ± 1.3	606.3 ± 3.3	29:71	
$Ru(phen)_3^{2+}$				0.38 ± 0.08

DNA cleavage activity. In order to evaluate the potential of L and L-Cu(II) as effective photosensitizer in PDT, we first tested their ability to damage DNA by means of gel electrophoresis experiments.

This method permits in fact, to distinguish the different conformational states of the biopolymer, upon drug-interaction, based on its relative mobility on the gel.(see ESI for further details). In particular the DNA plasmid, which is naturally occurring as a covalently closed circular or 'supercoiled' form (form I, ~2000 bp) and as an open circular form (~ 4000 bp), can be cleaved on one strand leading to the formation of a relaxed/nicked conformation (form II), that migrates approximately as the open circular form. In addition, more severe damages on DNA can provoke the cleavage of both strands of the biopolymer, leading to the formation of the linear form of DNA (form III), at~ 3000 bp.

The ability of **L** to damage the DNA plasmid upon light-activation, was evaluated by dosing plasmid pUC19 with increasing Ru(II) concentrations (0-100 μm) and analyzing the samples under dark and following irradiation Figures 6 a-bAs shown, no DNA cleavage occurs when the complex is kept under dark conditions. In fact, neither the supercoiled nor the open circular form of DNA undergo significant variations in the presence of the ruthenium compound, for the overall range of concentration tested.

Following photo-activation (Figure 6-b), a progressive conversion of the supercoiled form of DNA (form I) to the relaxed/nicked form (form II) was observed with increasing Ru(II) concentrations.

The dose-dependent DNA cleavage activity observed may indicate the capacity of L to produce photo induced single strand breaks (SSBs) on the plasmid.[47,48] This would be reasonably associated to its ability to produce singlet oxygen when light-activated, as discussed above..

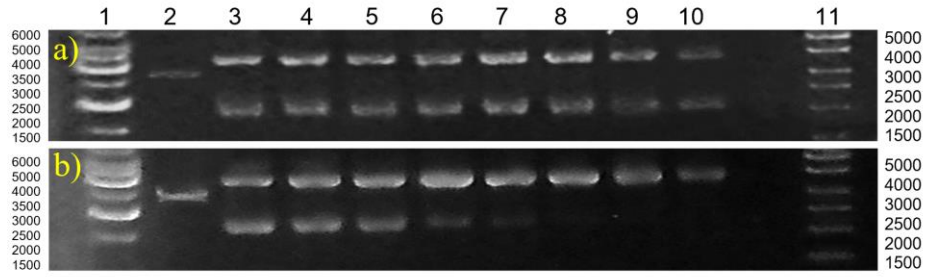

Figure 6. Agarose gels showing the dose response of **L** with 40 μg/ml pUC19 plasmid before (a) and after (b) 15 minutes of irradiation with visible light (λ > 450 nm, 200 W). Lanes 1 and 11, DNA molecular weight standard; lane 2, plasmid treated with EcoRI restrictase as control for linear DNA; lanes 3-10, 0, 1.56, 3.12, 6.25, 12.5, 25, 50, 100, μM of **L**.

An analogues study was performed on **L**-Cu(II) and results are reported in figure (figure 7-a--b). Under dark conditions, **L**-Cu(II) does not alter the natural conformations of DNA, at least in a range of Ru(II) concentrations within 0-25 μM (figure 7-a). For higher ruthenium concentrations, a conversion of the form I into form II was observed, indicating a nuclease activity of the copper complex itself.[49] Following irradiation (figure 7-b), a stronger oxidative damage on DNA was obtained, as revealed by the progressive formation of the linear form III of plasmid with increasing Ru(II) concentrations. This indicates the occurrence of double strand breaks (DSBs), more difficult to repair by restriction enzymes with respect to those provoked by SSBs,[50] in contrast with that obtained for L.

Besides the photo-activated experiments, we also evaluated the ability of L-Cu(II) to promote an oxidative damage on DNA under dark conditions, exploiting the presence of the fenton active metal center Cu(II). . To this aim, solutions of pUC19 containing increasing concentrations of **L**-Cu(II) (0-100 μM) were analyzed in the presence of a fixed concentration of hydrogen peroxide as co-reactant (50 μM, figure 7-c). As shown, a progressive conversion of the supercoiled form to the relaxed/nicked conformation, together with the formation of the linear form III, was observed with increasing concentration of compound.

In particular, above 12.5 μM of compound, form I undergoes an almost complete conversion to form II and form III, comparable to that obtained for the simultaneous presence of Cu(II) ion and H_2O_2 (control sample, lane 2 figure 7-b). This clearly evidences a straightened capacity of **L**-Cu(II) to produce both single and double strand breaks on DNA in presence of H_2O_2. With this regard, we can speculate that the copper ionwould be involved into Fenton or Fenton-like reactions with hydrogen peroxide (namely Cu(II) + H_2O_2 → Cu(I) + OH^- + $^{\bullet}OH$, see ESI for further details), leading to ROS production and thus providing an alternative mechanism for oxidative cleavage even in the absence of excitation by light.

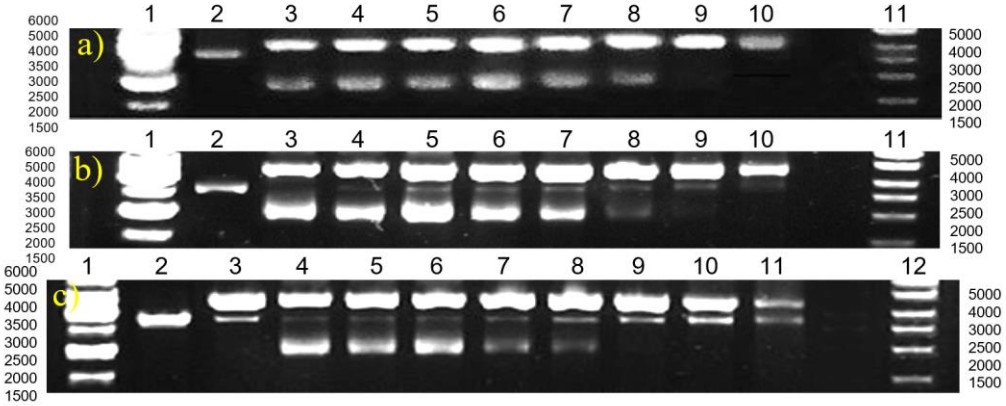

Figure 7. Agarose gels showing the dose response of **L**-Cu(II) with 40 μg/ml pUC19 plasmid before (a) and after (b) 15 minutes of irradiation with visible light (λ > 450 nm, 200 W). Lanes 1 and 11, DNA molecular weight standard; lane 2, plasmid treated with EcoRI restrictase as

control for linear DNA; lanes 3-10, 0, 1.56, 3.12, 6.25, 12.5, 25, 50, 100, μM of **L**-Cu(II). c) Agarose gel electrophoresis of **L**-Cu(II) with 40 μg/ml pUC19 in presence of H_2O_2 (50 μM). Lanes 1 and 12, DNA molecular weight standard; lane 2, linear pUC19; lane 3, plasmid treated with Cu(II) and H_2O_2 (100 μM each) and lanes 4-11, 0, 1.56, 3.12, 6.25, 12.5, 25, 50, 100, μM of **L**-Cu(II) complex.

***In vitro* studies.** Our further step in the investigation of the effective potential of **L** and **L**-Cu(II) to being used as possible drugs for PDT applications, was represented by the study of their cellular interaction. To this aim, we focused on the ability of Ru(II) compounds to interact with A375 human melanoma cell line, by means of Confocal Laser Scanning Microscopy (CLSM), and exploiting the classical luminescence of Ru(II) complexes with polypyridine.. A375 cells were incubated with **L** and **L**-Cu(II) by following the method described in the experimental;in Figure 8 are reported some representative CLSM images.

As shown in figures, cells treated with **L** and **L**-Cu(II) show several fluorescent spots into their cytoplasm and, in a less extent, inside the nuclei, indicating a good ability of both compounds to being internalized into the cellular compartments However, a comparison between the relative cellular penetration capacities is not completely reliable due to the scarce fluorescence emission of the copper complex with respect to L (ESI).

Interestingly, the ruthenium compounds appear to being not randomly distributed into the cellular cytosol but rather finely localized around the outer membrane of the nuclei. This let us to suggest that the cellular uptake of such compounds would be ruled by some specific endocytosis phenomena.

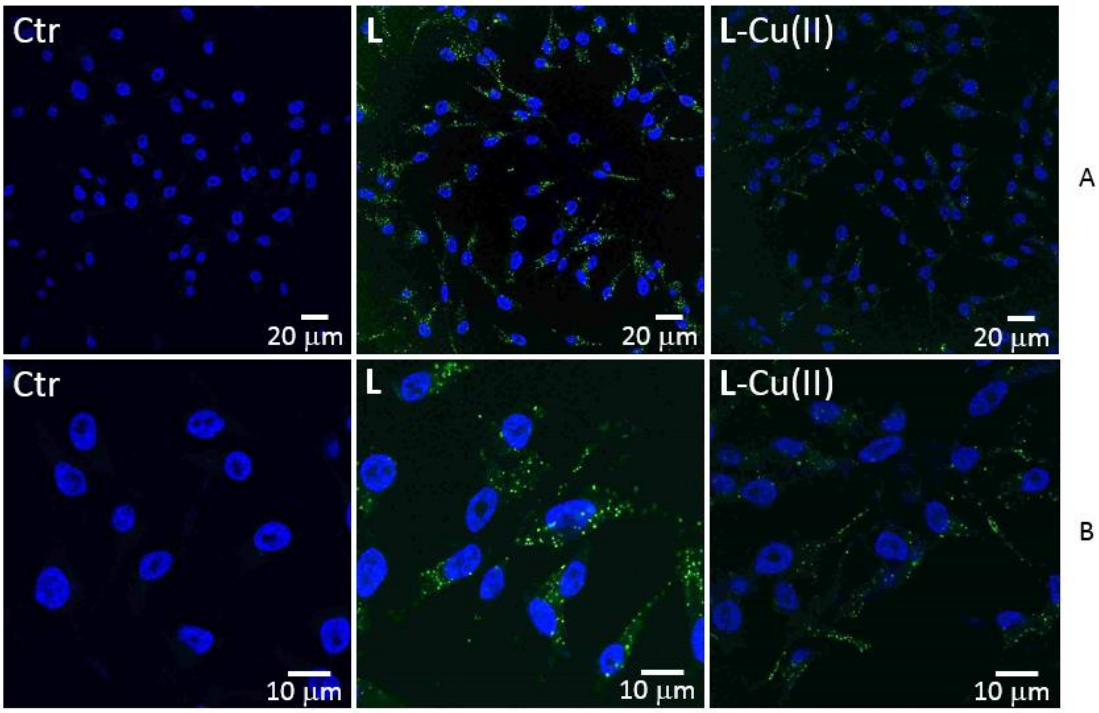

Figure 8. Fluorescence confocal microscopy imaging of A375 human melanoma cells incubated with **L** and **L**-Cu(II) (5μM each) for 24 hours. A and B show different magnifications of the images. DAPI (200 Nm, λ_{ex} 358 nm, λ_{em} 461 nm) was used to stain nuclei (blue spots) while in green is showed the fluorescence emission of **L** and **L**-Cu(II) respectively (λ_{ex} 440-480 nm, λ_{em} 600-640 nm).

Finally, the ability of **L** and **L**-Cu(II) to induce cell death after exposition to light, was evaluated through MTT assay on A375 cell line. In Figure 9a-b are reported the viability titres of A375 cells treated with different concentrations of **L** and **L**-Cu(II) respectively, measured before (black bars) and upon (grey bars) irradiation. As shown, the viability of cells not exposed to light is comparable to that of controls, for both the compounds, thus demonstrating that **L** and **L**-Cu(II) are no toxic under dark conditions being well tolerated by cells.

Following photo-activation Figure 9a-b (grey bars), we observed a different behaviour for **L** and **L**-Cu(II).In particular **L**, despite its capacity to produce $^1O_2$ upon light-activation, results to be effective in reducing the cell viability only for dosage higher than 5 μM. Of note, a greater

photo-induced cytotoxicity was observed for **L**-Cu(II), which is effective even at lower concentrations (0.25 μM) and features dose-dependent activity. .

This finding can be rationalized considering the key role of the copper(II) ion within the macrocyclic cavity L'. Based on these data in fact, we can speculate that the fenton-active copper center plays a synergetic role with light activation in the development of cytotoxic ROS species, providing additional mechanisms for the oxidative damage to biological targets.

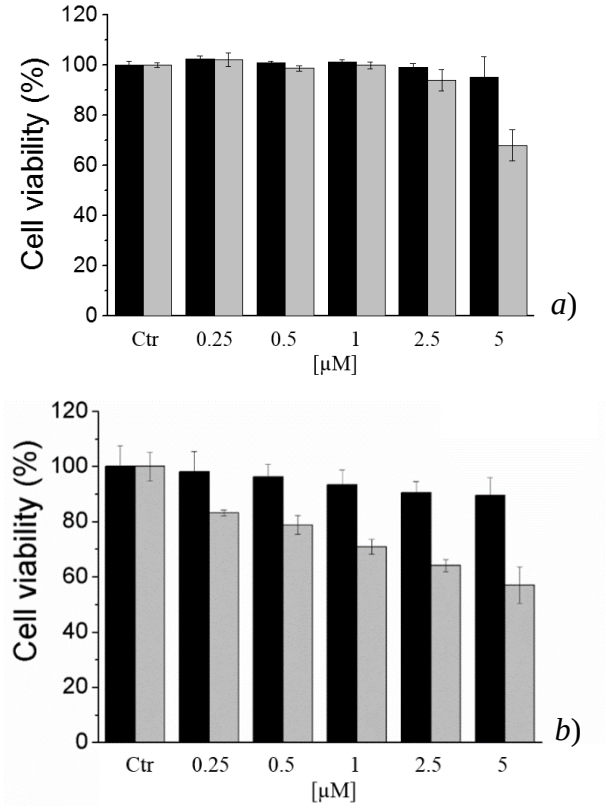

Figure 9. Cell viability assays of A375 human melanoma cells treated with increasing concentrations of **L** (*a*) and **L**-Cu(II) (*b*) measured before (black bars) and upon light irradiation (grey bars).

EXPERIMENTAL SECTION

Materials. All materials were of reagent grade and used without further purification. The synthesis of 4,4'-(2,5,8,11,14-pentaaza[15])-2,2'-bipyridilophane (**L'**) was described in a previous paper.[29]

Calf thymus DNA (ct-DNA) was purchased from Sigma Aldrich as sodium salt. Solutions of ct-DNA were obtained by dissolving it in Tris-HCl buffer (5 mM Tris-HCl, 50 mM NaCl, pH = 7.2). The purity of DNA was assessed by UV absorption measurements; a UV absorbance ratio at 260 and 280 nm of about 1.8-1.9:1, indicates that DNA was sufficiently free of protein.[51] The DNA concentration per nucleotide was determined by absorption spectroscopy using the molar absorption coefficient 6600 $M^{-1}cm^{-1}$ at 260 nm.[52]

Synthesis of $[Ru(phen)_2L']Cl_2$ (L). Equimolar amounts of $Ru(phen)_2Cl_2$ and **L'** (0.24 mmol) were suspended in 9.6 ml of ethylene glycol. After sonication to facilitate the dispersion of reagents into the solvent, the mixture was heated in a microwave reactor (300 W) for 7 minutes at 160 °C. The dark-violet suspension became a deep orange solution. After being cooled at room temperature, the solvent was removed by distillation at low pressure, and the residue was dissolved in the minimal amount of HCl 6 M. Water was completely removed by evaporating the solution under reduced pressure. Ethanol was added and the resulting red-orange suspension was collected by filtration and washed with acetone/ethyl ether. The product, obtained as penta-hydrochloride salt, was recrystallized twice from ethanol, washed with ethyl ether and dried on H_2SO_4 97%. Anal. Found: C, 47.3; H, 5.1; N, 13.7. Calcd. for $C_{44}H_{56}Cl_7N_{11}RuO_2$: C, 47.18; H, 5.04; N, 13.75. ^{1}H-NMR (D_2O + DCl, pD < 2, 400 MHz, Bruker ARX-400): δ(ppm) 8.91 (s, 2H, L', 3,3'); 8.66 (d, 2H, L', 6, 6'); 8.53 (d, 2H); 8.28 (d, 2H); 8.21 (m, 4H); 7.91 (d, 2H, L', 5,5');

7.85 (d, 2H); 7.79 (m, 2H); 7.52 (m, 2H); 7.31 (d, 2H); 4.59 (m, 4H, L', pyCH_2N); 3.65 (m, 16H, L', NCH_2CH_2N). ^{13}C-NMR (D_2O, pD < 2, 400 MHz, Bruker ARX-400): δ(ppm): 152.5, 152.3, 151.8, 148.3, 147.6, 146.9, 137.0, 136.8, 133.7, 130.9, 127.8, 127.49, 127.1, 126.7, 125.9, 125.3, 123.1. ESI-MS: [M^+] m/z = 831.3; [M^{2+}] m/z = 415.65. Yield: 234.4 mg, 0.18 mmol (75%).

Synthesis of [CuRu(phen)$_2$L'](ClO_4)$_4$·4H_2O.

A 10 ml of aqueous solution of $Cu(ClO_4)_2·6H_2O$ (7.50 mg, 0.020 mmol) was added to a solution of **L**$Cl_2·5HCl·2H_2O$ (22.5 mg, 0.020 mmol) in 25 ml of water. The pH was adjusted to 6.5 with NaOH 0.1 and $NaClO_4$ (100 mg) was added. The solution was stirred at room temperature for 1h. A blue powder of Cu**L**$(ClO_4)_4·4H_2O$ was formed by slow evaporation. Yield: 23 mg (85%). Elem. Anal. Calc. for $C_{44}H_{55}N_{11}RuCuCl_4O_{20}$: C, 38.68; H, 4.06; N, 11.28. Found: C, 38.6; H, 4.1; N, 11.2%.

Potentiometric measurements. Equilibrium constants for protonation and metal ion binding of **L** were determined by means of potentiometric measurements (pH = -log [H^+]), carried out in degassed 0.1 M NaCl at 298.1 ± 0.1 K, by using equipment and procedures which have been already described.[53]

The reference electrode was an Ag/AgCl electrode in saturated KCl solution. The glass electrode was calibrated as a hydrogen concentration probe by titrating known amounts of HCl with CO_2-free NaOH solutions and the equivalent point was determined by using the Gran's method.[54] Through this process we determined the standard potential E_o, as well as the ionic product of water (pK_w = 13.73 ± 0.01 at 298.1 K in 0.1 M NaCl). Three titration experiments (consisting of 100 data points for each one) were performed in the pH range 1.5 -12.

A ligand concentration of about 1 x 10^{-3} M was generally employed. In Zn(II) titrations a metal ion concentration of 0.8[**L**] was used while in the case of Cu(II) its concentration varied from 0.8[**L**] to 1.8[**L**]. The computer program HYPERQUAD[55] was used to determine both protonation and complexation (metal ions) constants of the ligand from e.m.f. data.

Electronic absorption and fluorescence measurements. Absorption spectra were registered on a Perkin-Elmer Lambda 6 spectrophotometer. Fluorescence spectra were recorded on a Perkin-Elmer LS55 spectrofluorimeter, by using an excitation wavelength of 411 nm. All measurements were performed at 298.0 ± 0.1 K by using solutions of ligand in Tris-HCl buffer (5 mM, NaCl 50 mM, pH = 7.2). Absorption and fluorescence titration of Ru(II) complexes with ct-DNA were carried out and data analyzed as described in details in the supporting information.

Excited state lifetime measurements. Excited state lifetime measurements were perfomed by using a 50 μM solution of **L** in Tris-HCl Buffer (pH 7.2), in a fused silica 10 mm path length cuvette. Measurements were carried out in backscattering geometry, where the 532 nm radiation, corresponding to the second harmonic of a Nd:YAG pulsed laser, was focused on the cuvette and the fluorescence radiation was collected by a lens and focalized on the slit of a monochromator (Princeton Instruments Acton 2300i) passing through a notch filter to suppress the backscattered laser radiation. The dispersed fluorescence spectra were detected by an air-cooled CCD. The time variable was introduced using a pulsed detection. The CCD detector was activated with a high voltage pulse of 5 ns time width, starting 20 ns before the laser pulse up to 2280 ns after, for a total time of 2300 ns. For each sample, 461 fluorescence spectra were registered and entirely

integrated. The fluorescence decay curves were obtained by reporting in a graph the integrated intensity values versus the time delay with respect to the laser pulse.

The same procedure was followed for both the free ruthenium complex and that containing 20 equivalents of ct-DNA. The excited decay profiles for L with DNA were fitted to biexponential decay curves while a single exponential decay fit was applied in the applied in the case of the free ruthenium complex.

Singlet oxygen detection. The emission from $^1O_2$ at 1270 nm induced by laser excitation of the ruthenium-based systems was used to determine the relative $^1O_2$ quantum yields values (ϕ_Δ) in CH_3CN air-saturated solutions. In all the experiments the laser source was a Ti-Sapphire ultrafast laser delivering 100 fs long pulses at 82 MHz repetition rate and 800 nm wavelength. The laser pulse was frequency doubled at 400 nm to excite the solutions. Tetraphenylporphyrin (TPP) was chosen as reference standard while $Ru(phen)_3$ was included in our experiments in order to compare the $^1O_2$ quantum yields of **L** and **L**-Cu(II) with a parental compound featuring analogue chemical makeup of the ruthenium center. All samples were dissolved in acetonitrile and held in 1 cm path quartz cuvettes. Samples were saturated with air and no O_2 was insufflated in the solutions. $^1O_2$ emission was collected by a lens set at 90° with respect to the 400 nm exciting laser beam and focused on a N_2 cooled InGaAs photodiode. To select $^1O_2$ emission an interference filter centered at 1270 ± 20 nm was placed in front of the photodiodie. A chopper working at 90 Hz was placed on the exciting beam and used to trigger a lock-in amplifier, which singled out and averaged the signal from the photodiode. In order to verify that only singlet oxygen emission was measured by the experimental set-up all the sample solutions were degassed through pump-freeze-thow cycles in quartz tubes sealed under vacuum and no signal

from these samples was observed. Experiments were run on solutions of different concentration with absorbance values at 400 nm in the range 0.08 – 0.2 and with increasing applied laser power. Linearity with respect to applied laser power was observed. The $^1O_2$ quantum yields of samples (*S*) were calculated with the formula:

$$\phi_\Delta(S) = \phi_\Delta(R)\frac{s(S)x\left[1-10^{-A(R)}\right]}{s(R)x\left[1-10^{-A(S)}\right]} \qquad (2)$$

where ϕ_Δ (*S*) and ϕ_Δ (*R*) represents the $^1O_2$ quantum yields of samples and the reference respectively, *s* is the slope of the linear plot of the intensity of $^1O_2$ luminescence signal as a function of the intensity of the exciting laser, and *A*(*R*/*S*) represents the absorbance at 400 nm for the *R*/*S* solutions. A ϕ_Δ value of 0.60 was used for TPP, as reported by R. Schmidt and E. Afshari by chemical methods in acetonitrile.[56]

Gel electrophoresis experiments. The ability of Ru(II) compounds to damage DNA, was tested by using the puC-19 plasmid. The DNA forms were resolved on 1% agarose gel in Tris-Acetate-EDTA buffer (TAE, pH 8). Experiments were performed by dosing the plasmid with increasing concentrations of Ru(II) compounds. Typically, each sample was prepared by adding 10 µl of a concentrated solution of the ruthenium compounds (**L** or **L**-Cu(II), pH 7.4), to 10 µl of puC-19 (80 µg/ml) in order to obtain final concentrations of ruthenium and pUC-19 of 0-100 µM and 40 µg/ml respectively, in a total volume of 20 µl. After mixing, the samples were incubated at 37 °C for 30 minutes. As markers were used Gene ruler DNA (1kb) and mass ruler high range DNA ladders, while as control for double strand breaks, a reference plasmid sample was linearized with EcoRI endonuclease (Fast digest EcoRI, Fermentas). The inactivation of EcoRI, was obtained by keeping the temperature at 80 °C for 5 minutes. 6 µl of each sample, 3 µl of milliQ

water and 1 µl of Fast Digest Green Buffer 10X, as DNA loading dye, were mixed together. The resulting samples were run for 45 minutes at 100 mV and the gels were finally analyzed with a trans-Uv illuminator.

Photodynamic experiments were performed before and after 15 minutes of irradiation with visible light ($\lambda > 450$ nm) of samples containing DNA and the ruthenium complexes (**L** and **L**-Cu(II)) at increasing molar concentrations. The DNA-cleavage like activity of **L**-Cu(II) was instead investigated by performing the experiments in the absence and in the presence of 50 µM of H_2O_2, under dark conditions.

Flow cytometry and confocal microscopy. A 375 human melanoma cells (1×10^5) were seeded in p35 well and incubated with **L** and **L**-Cu(II) (5µM) for 24 h. Then cells were extensively washed with PBS, trypsinized and pelleted by centrifugation in conical 15 ml tubes. Cells were analysed by a FACS-Canto-II flow cytometer (BD Biosciences, San Jose, CA, USA) and data were analysed with the FACSDiva (Ashland, OR, USA) software. For each samples 1 x 10^4 events were acquired.

For confocal microscopy, cells were plated on glass cover slips and incubated with **L** and **L**-Cu(II) (5µM) for 24 h. Then they were washed with PBS and fixed with 3% formaldheyde solution in PBS for 20 min at room temperature. After extensive washing in PBS, the cells were permeabilized with 0.1% TritonX100 (Sigma) and subsequently incubated with DAPI Molecular Probes (200 nM, λ_{ex}. 358 nm, λ_{em}. 461 nm) to stain nuclei. The cells were mounted with glycerol plastine and observed under a laser-scanning confocal microscope (LeicaSP8).

Cell viability. Cell viability was evaluated by using the MTT method. Briefly, A375 cells (1x 10^4) were seeded on 24 multiplate well, and the incubated in the presence of increasing compound concentrations. For each compound (**L** or **L**-Cu(II)) two plates were prepared: the first was used as control test and was maintained in the dark, while the latter was exposed to light. After 24 hours incubation, cells treated with **L** and **L**-Cu(II) were exposed to light for 15 minutes, using a 60 watts light positioned at 4 cm distance from plate. After radiation, plates were stored for further 48 h at 37°C. Finally, cell viability was assayed incubating cells in the presence of 0.5 mg/ml of 3-(4,5-dimethylthiazol-2-yl)-2,5-diphenyltetrazolium bromide salt for 1 hour. Then, cells was washed with PBS and lysed using DMSO solution, to dissolve insoluble formazan crystals produced by viable cells. The absorbance of solutions obtained was determined by using a microplate readers *(*Model 550 Microplate Reader, Biorad, USA)

CONCLUSION

In conclusion, we report on the synthesis and chemical-physical characterization of two new, higly water soluble, Ru(II) and Ru(II)/Cu(II) polypyridyl complexes containing the peculiar polyamino-macrocycle unit L'. Both compounds were found to effectively interact with ct-DNA, as emerged from Uv-visible and fluorescence measurements. Our studies on pUC19 point out their capacity to cleave the macromolecule under light irradiation. In particular, while L is able to produce photo induced single strand breaks (SSBs) on plasmid, reasonably due to singlet

oxygen generation, the presence of Cu(II) ion in L-Cu(II) determines the formation of more severe double strand breaks (DSBs). Exploiting the classic luminescence of Ru(II) polypyridine complexes, L and L-Cu(II), even in the presence of Cu(II), can be visualized in cells, revealing a high tendency to be internalized into cellular compartments of A375 human melanoma cell line. Moreover, both compounds are no-toxic under dark conditions but display an enhanced cytotoxicity when exposed to light. In particular, L-Cu(II) shows a greater photo-induced dose dependent cytotoxicity with respect to L, remarking the key role of the Cu(II) metal center in the polyaminomacrocyclic unit. Despite further studies need to be performed in order to deeply characterize the cytotoxic species involved in the oxidative pathways originated from photo-activation of L-Cu(II), these results suggest that the fenton-active copper center plays a synergetic role with light activation in the development of ROS species. In conclusion, the polyamine unit represents an added value to these potential PS agents, affording the formation of mixed Ru(II)/Cu(II) complexes featuring additional/alternative mechanisms for the oxidative damage of biological targets with respect to the sole singlet oxygen production.

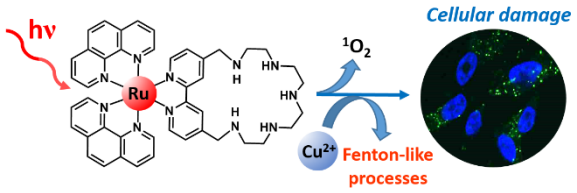

Novel Ru(II) and Ru(II)/Cu(II) mixed polypyridyl complexes featuring different light-activated mechanisms; singlet oxygen generation and fenton-like oxidative pathways.

References

1 E. J. Dennis, G. J. Dolmans, D. Fukumura and K. J. Rakesh, *Nat. Rev. Cancer*, 2003, **3**, 380–387.

2 Z. Zhou, J. Song, L. Nie and X. Chen, *Chem. Soc. Rev.*, 2016, **45**, 6597–6626.

3 J. P. Celli, B. Q. Spring, I. Rizvi, C. L. Evans, K. S. Samkoe, S. Verma, B. W. Pogue and T. Hasan, *Chem. Rev.*, 2010, **110**, 2795–2838.

4 G. Boccalini, L. Conti, C. Montis, D. Bani, A. Bencini, D. Berti, C. Giorgi, A. Mengoni and B. Valtancoli, *J. Mater. Chem. B*, 2017, **5**, 2788–2797.

5 J. Hess, H. Huang, A. Kaiser, V. Pierroz, O. Blacque, H. Chao and G. Gasser, *Chem. - A Eur. J.*, 2017, **23**, 9888–9896.

6 A. P. Castano, T. N. Demidova and M. R. Hamblin, *Photodiagnosis Photodyn Ther*, 2004, **1**, 279–293.

7 C. Mari, V. Pierroz, S. Ferrari and G. Gasser, *Chem. Sci.*, 2015, **6**, 2660–2686.

8 K. Plaetzer, B. Krammer, J. Berlanda, F. Berr and T. Kiesslich, *Lasers Med. Sci.*, 2009, 24, 259–268.

9 J. Zhang, C. Jiang, J. P. Figueiró Longo, R. B. Azevedo, H. Zhang and L. A. Muehlmann, *Acta Pharm. Sin. B*, 2018, **8**, 137–146.

10 L. B. Josefsen and R. W. Boyle, *Met. Based. Drugs*, 2008, 2008.

11 P. Alreja and N. Kaur, *Inorg. Chem. Commun.*, 2017, **77**, 51–54.

12 L. Zeng, P. Gupta, Y. Chen, E. Wang, L. Ji, H. Chao and Z. S. Chen, *Chem. Soc. Rev.*,

2017, 46, 5771–5804.

13 A. Li, C. Turro and J. J. Kodanko, *Acc. Chem. Res.*, 2018, **51**, 1415–1421.

14 K. Zheng, Q. Wu, C. Wang, W. Tan and W. Mei, *Anticancer. Agents Med. Chem.*, 2017, **17**.

15 J. W. Dobrucki, *J. Photochem. Photobiol. B Biol.*, 2001, **65**, 136–144.

16 V. Brabec and J. Kasparkova, *Coord. Chem. Rev.*, 2018, 376, 75–94.

17 H.-J. Yu, S.-M. Huang, L.-Y. Li, H.-N. Jia, H. Chao, Z.-W. Mao, J.-Z. Liu and L.-N. Ji, *J. Inorg. Biochem.*, 2009, **103**, 881–890.

18 M. Klajner, C. Licona, L. Fetzer, P. Hebraud, G. Mellitzer, M. Pfeffer, S. Harlepp and C. Gaiddon, *Inorg. Chem.*, 2014, **53**, 5150–5158.

19 E. V. Bichenkova, X. Yu, P. Bhadra, H. Heissigerova, S. J. A. Pope, B. J. Coe, S. Faulkner and K. T. Douglas, *Inorg. Chem.*, 2005, **44**, 4112–4114.

20 P. D. Beer and J. Cadman, *New J. Chem.*, 1999, **23**, 347–349.

21 T. E. Keyes, J. G. Vos, J. A. Kolnaar, J. G. Haasnoot, J. Reedijk and R. Hage, *Inorganica Chim. Acta*, 1996, **245**, 237–242.

22 E. Wachter, D. K. Heidary, B. S. Howerton, S. Parkin and E. C. Glazer, *Chem. Commun.*, 2012, **48**, 9649.

23 K. A. Kaphingst, S. Persky and C. Lachance, 2010, **14**, 384–399.

24 J. Cao, Q. Wu, W. Zheng, L. Li and W. Mei, *RSC Adv.*, 2017, **7**, 26625–26632.

25 C. Lodeiro, F. Pina, A. J. Parola, A. Bencini, A. Bianchi, C. Bazzicalupi, S. Ciattini, C. Giorgi, A. Masotti, B. Valtancoli and J. Seixas de Melo, *Inorg. Chem.*, 2001, **40**, 6813–6819.

26 A. Bencini, A. Bianchi, E. Garcia-España, M. Micheloni and J. A. Ramirez, *Coord. Chem. Rev.*, 1999, **188**, 97–156.

27 F. Bettazzi, D. Voccia, A. Bencini, C. Giorgi and I. Palchetti, .

28 Z. Murtaza, Q. Chang, G. Rao, H. Lin and J. R. Lakowicz, *Anal. Biochem.*, 1997, **222**, 216–222.

29 C. Lodeiro, A. J. Parola, F. Pina, C. Bazzicalupi, A. Bencini, A. Bianchi, C. Giorgi, A. Masotti and B. Valtancoli, *Inorg. Chem.*, 2001, **40**, 2968–2975.

30 A. M. Josceanu, P. Moore, S. C. Rawle, P. Sheldon and S. M. Smith, 1995, **240**, 159–168.

31 Y. J. Liu, H. Chao, L. F. Tan, Y. X. Yuan, W. Wei and L. N. Ji, *J. Inorg. Biochem.*, 2005, **99**, 530–537.

32 T. Nandhini, K. R. Anju, V. M. Manikandamathavan, V. G. Vaidyanathan and B. U. Nair, *Dalt. Trans.*, 2015, **44**, 9044–9051.

33 A. M. Pyle, J. P. Rehmann, R. Meshoyrer, C. V. Kumar, N. J. Turro and J. K. Barton, *J. Am. Chem. Soc.*, 1989, **111**, 3051–3058.

34 P. Lincoln and B. Norden, *Doktorsavhandlingar vid Chalmers Tek. Hogsk.*, 1998, 9583–9594.

35 S. Satyanarayana, J. C. Dabrowiak and J. B. Chaires, *Biochemistry*, 1993, **32**, 2573–2584.

36 M. Eriksson, M. Leijon, C. Hiort, B. Norden and A. Graeslund, *J. Am. Chem. Soc.*, 1992, **114**, 4933–4934.

37 C. Turro, S. H. Bossmann, Y. Jenkins, J. K. Barton and N. J. Turro, *J. Am. Chem. Soc.*, 1995, **117**, 9026–9032.

38 A. E. Friedman, J. K. Barton, J. C. Chambron, J. P. Sauvage, N. J. Turro and J. K. Barton, *J. Am. Chem. Soc.*, 1990, **112**, 4960–4962.

39 J. K. Barton, A. T. Danishefsky and J. M. Goldberg, *J. Am. Chem. Soc.*, 1984, **106**, 2172–2176.

40 L. Li, H. M. Liu, X. K. Liu, S. Y. Liao, Y. T. Lan, Q. Wu, X. C. Wang, Q. Wang, S. Y. Zhang and W. J. Mei, *RSC Adv.*, 2017, **7**, 23727–23734.

41 D. Wang, J. Wang, D. Moses, G. C. Bazan and A. J. Heeger, *Langmuir*, 2001, **17**, 1262–1266.

42 M. R. Eftink and L. A. Selvidge, *Biochemistry*, 1982, **21**, 117–125.

43 R. E. Holmlin, E. D. a. Stemp and J. K. Barton, *Inorg. Chem.*, 1998, **37**, 29–34.

44 D. Z. M. Coggan, I. S. Haworth, P. J. Bates, A. Robinson and A. Rodger, *Inorg. Chem.*, 1999, **38**, 4486–4497.

45 J. K. Barton, J. M. Goldberg, C. V Kumar and N. J. Turro, 1986, 2081–2088.

46 S. J. Moon, J. M. Kim, J. Y. Choi, S. K. Kim, J. S. Lee and H. G. Jang, *J. Inorg. Biochem.*, 2005, **99**, 994–1000.

47 B. S. Howerton, D. K. Heidary and E. C. Glazer, *J. Am. Chem. Soc.*, 2012, **134**, 8324–8327.

48 F. Wang and H. Chao, *Helv. Chim. Acta*, 2007, **90**, 205–215.

49 P. U. Maheswari, S. Roy, H. Den Dulk, S. Barends, G. Van Wezel, B. Kozlevčar, P. Gamez and J. Reedijk, *J. Am. Chem. Soc.*, 2006, **128**, 710–711.

50 F. V. Pamatong, C. A. Detmer and J. R. Bocarsly, *J. Am. Chem. Soc.*, 1996, **118**, 5339–5345.

51 J. Marmur, *J. Mol. Biol.*, 1961, **3**, IN1-218.

52 M. E. Reichmann, S. A. Rice, C. A. Thomas and P. Doty, *J. Am. Chem. Soc.*, 1954, **76**, 3047–3053.

53 C. Bazzicalupi, A. Bianchi, C. Giorgi, P. Gratteri, P. Mariani and B. Valtancoli, *Inorg. Chem.*, 2013, **52**, 2125–2137.

54 G. Gran, *Analyst*, 1952, **77**, 661.

55 P. Gans, A. Sabatini and A. Vacca, *Talanta*, 1996, **43**, 1739–1753.

56 R. Schmidt and E. Afshari, *J phys Chem*, 1990, **94**, 4377–4378.

57 F. Wang, J. Xu, K. Wu, S. K. Weidt, C. L. MacKay, P. R. R. Langridge-Smith and P. J. Sadler, *Dalt. Trans.*, 2013, **42**, 3188–3195.

58 H. Chen, J. A. Parkinson, R. E. Morris and P. J. Sadler, *J. Am. Chem. Soc.*, 2003, **125**, 173–186.

59 B. J. Pages, D. L. Ang, E. P. Wright and J. R. Aldrich-Wright, *Dalt. Trans.*, 2015, **44**, 3505–3526.

60 C. Hiort, B. Norden and A. Rodger, *J. Am. Chem. Soc.*, 1990, **112**, 1971–1982.